CCR7 ligands control basal T cell motility within lymph node slices in a phosphoinositide 3–kinase–independent manner

François Asperti-Boursin,[1,2] Eliana Real,[1,2] Georges Bismuth,[1,2] Alain Trautmann,[1,2] and Emmanuel Donnadieu[1,2]

[1]Institut Cochin, Université Paris Descartes, Centre National de la Recherche Scientifique (UMR 8104), F-75014 Paris, France
[2]Institut National de la Santé et de la Recherche Médicale, U567, F-75014 Paris, France

The molecular mechanisms responsible for the sustained basal motility of T cells within lymph nodes (LNs) remain elusive. To study T cell motility in a LN environment, we have developed a new experimental system based on slices of LNs that allows the assessment of T cell trafficking after adoptive transfer or direct addition of T cells to the slice. Using this experimental system, we show that T cell motility is highly sensitive to pertussis toxin and strongly depends on CCR7 and its ligands. Our results also demonstrate that, despite its established role in myeloid cell locomotion, phosphoinositide 3–kinase (PI3K) activity does not contribute to the exploratory behavior of the T lymphocytes within LN slices. Likewise, although PI3K activation is detectable in chemokine-treated T cells, PI3K plays only a minor role in T cell polarization and migration in vitro. Collectively, our results suggest that the common amplification system that, in other cells, facilitates large phosphatidylinositol 3,4,5-trisphosphate increases at the plasma membrane is absent in T cells. We conclude that T cell motility within LNs is not an intrinsic property of T lymphocytes but is driven in a PI3K-independent manner by the lymphoid chemokine-rich environment.

CORRESPONDENCE
Emmanuel Donnadieu:
donnnadieu@cochin.inserm.fr

Abbreviations used: CCL and CCR, CC chemokine ligand and receptor, respectively; CMFDA, 5-chloromethylfluorescein diacetate; CXCL, CXC chemokine ligand; DOCK2, dedicator of cytokinesis 2; FRC, fibroblastic reticular cell; GEF, guanine nucleotide exchange factor; HEV, high endothelial venule; PBT cell, peripheral blood T cell; PH, pleckstrin homology; PI3K, phosphoinositide 3–kinase; PIP3, phosphatidylinositol 3,4,5-trisphosphate; *plt*, *paucity of LN T cell*; PTX, pertussis toxin; WMN, wortmannin.

Effective immune surveillance relies on continuous migration of T lymphocytes between the blood, lymph circulation, and secondary lymphoid organs. The recruitment of naive T cells in LNs is a multistep process that depends on chemokines, among which the CC chemokine receptor (CCR) 7 ligands CCL19 and CCL21 play a crucial role. Indeed, CCL21 is expressed by high endothelial venules (HEVs) (1), and both CCL19 and CCL21 are present in the LN T cell zone (for review see reference 2). Mice homozygous for a spontaneous mutation, *paucity of LN T cell* (*plt*), that lack CCL19 and CCL21 expression in lymphoid organs have defective T cell trafficking into LNs (3). In addition, T cells from CCR7-deficient mice fail to home to LNs (4). These convergent studies point to the importance of CCR7 for T cell migration across HEVs.

After T cells have transmigrated through the vessel walls of HEVs, they further migrate within the LNs. Since 2002, several studies performed by two-photon microscopy have revealed that within LNs, T cells display a highly motile behavior, which allows them to scan from several hundred to several thousand antigen-presenting cells per hour (5, 6). The nature of the molecules responsible for this intense T cell trafficking in vivo is an area of intense interest. It has recently been shown that within LNs, T cells migrate almost exclusively along networks of a stromal cell type localized in the T zone, the fibroblastic reticular cell (FRC) (7). The role of chemokines in this process has been hypothesized but not yet demonstrated (8). In addition, genetic approaches have led to the conclusion that Gαi was required for normal B cell motility within LNs (9). Consistent with a similar control of intranodal T cell motility, our previous in vitro studies showed that human DCs were able to trigger naive T cell motility through the secretion of CCL19 (10). In addition, besides CCR7 ligands, other chemokines that are constitutively expressed in LNs, such as CXC chemokine ligand (CXCL)

F. Asperti-Boursin and E. Real contributed equally to this work.
The online version of this article contains supplemental material.

12, could contribute to steady-state T cell motility. However, the involvement of CCR7 and CXCR4 ligands in controlling T cell motility within LNs has not been formally proven, and we ignore whether other chemokines contribute to this phenomenon.

To better understand how T cell motility is controlled in LNs, we need not only to assess the role of chemokines and identify the important ones, but also to clarify the nature of the intracellular signaling pathways that control cell polarization and motility within LNs. From amoebas to fibroblasts and neutrophils, phosphoinositide 3–kinase (PI3K) plays an evolutionary conserved role in the control of cell migration and in instructing where the actin polymerizing machinery should be active (11). Among the different PI3K isoforms, PI3Kγ is particularly relevant for neutrophil migration. However, other PI3K isoforms contribute to the production of 3′-phosphoinositides in these cells as part of a Rac-dependent positive-feedback loop initiated downstream of G protein–coupled receptors (12, 13).

In lymphocytes, a few reports show that the importance of PI3K for chemokine signaling is less marked than in neutrophils. T cell migration in a gradient of CCL21 or CXCL12 is only partially reduced by the PI3K inhibitor wortmannin (WMN) (14, 15). An important part of the PI3K-independent signaling pathway that controls chemokine-induced T cell migration depends on dedicator of cytokinesis 2 (DOCK2), an unconventional guanine nucleotide exchange factor (GEF) for Rac (15). However, most of these studies have been performed in vitro, and the importance of PI3K in T cell migration within the LNs remains unsettled.

To better understand the molecular mechanisms underlying T cell polarization and motility, we initially examined the role of PI3K in various aspects of chemokine signaling in vitro. We demonstrate the absence of a 3′-phosphoinositide amplification loop downstream of chemokine receptors, which prevents massive PI3K activation after chemokine signaling, contrary to what is observed in the same cells after stimulation with an antigen-presenting cell (16). This probably explains the minor role played by PI3K in chemokine-induced T cell polarization, motility, and migration. We have also developed an excised LN slice preparation in which one can analyze, in a physiologically relevant three-dimensional structure, not only the identity of chemokines controlling T cell motility, but also signaling events such as the role of PI3K. We have established that T cell motility within this preparation was dependent on the action of the lymphoid chemokines CCL21 and CCL19.

RESULTS

A phosphatidylinositol 3,4,5-trisphosphate (PIP3)–specific probe is not recruited to the plasma membrane during T lymphocyte migration

We have used the pleckstrin homology (PH) domain of AKT fused to CFP (17) to visualize the pattern of PI3K activity in T lymphocytes as they polarized and migrated on immobilized ICAM-1 after CCL19 stimulation. T cells were cotransfected with AKT-PH-CFP and YFP, a fluorescent cytosolic marker used as a reference to normalize the AKT-PH-CFP signal. In unstimulated T cells, the CFP/YFP ratio was homogeneous throughout cytosol and nuclei, attesting

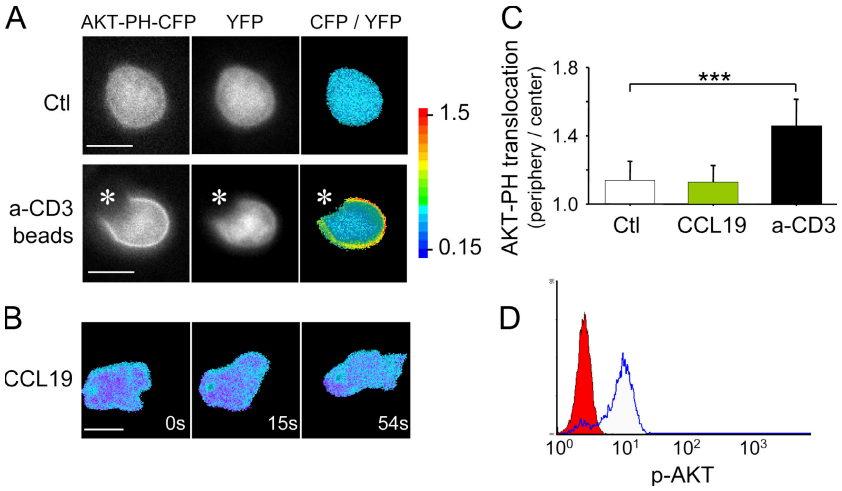

Figure 1. Absence of PIP3 gradients in motile T cells. (A) Human PBT cells were cotransfected with AKT-PH-CFP and YFP and were either left unstimulated or stimulated with anti-CD3/CD28–coated beads, as indicated by an asterisk. (right) The ratio of PH-CFP/YFP is shown as a pseudocolored image. Bar, 5 μm. (B) Ratiometric measurement of PIP3 in representative migrating T cells. The same conditions as in A were used, except that T cells were plated on ICAM-1–coated coverslips and stimulated with 100 ng/ml of soluble CCL19. A time-lapse animation of this cell is shown in Video 1. Bar, 5 μm. Data in A and B are representative of three experiments. (C) Quantification of AKT-PH enrichment to the cell periphery in unstimulated (Ctl), anti-CD3/CD28–stimulated, and CCL19-stimulated cells migrating on ICAM-1. Data are the means ± SD of 18–34 cells per condition in three independent experiments. ***, $P < 0.001$. (D) AKT phosphorylation triggered by soluble CCL19. PBT cells were stimulated as in A, fixed, stained with anti–P-AKT (Ser473), and analyzed by flow cytometry. The y axis corresponds to the number of T cells. Unstained T cells are represented in red, and stained T cells are represented in blue. Video 1 is available at http://www.jem.org/cgi/content/full/jem.20062079/DC1.

to the absence of basal PI3K activity in resting T cells (Fig. 1 A, top). As a positive control, we used polystyrene beads coated with anti-CD3 and anti-CD28 that mimic an antigen-specific stimulation. Under this condition, the ratio of CFP/YFP was clearly increased at the cell periphery in every cell contacting a bead (Fig. 1 A, bottom). A translocation index was calculated (see Materials and methods) to quantify the AKT-PH enrichment at the cell periphery. As shown in Fig. 1 C, in unstimulated cells, the mean index was 1.14 ± 0.11 (mean ± SD; $n = 31$), whereas in cells stimulated with beads, this index increased to 1.45 ± 0.16 ($n = 18$; $P < 0.001$). Surprisingly, in T cells migrating in the presence of CCL19, the mean index (1.13 ± 0.1; $n = 34$) was identical to that observed in unstimulated T cells even though AKT phosphorylation, another readout of PI3K activation, was readily measured by flow cytometry and maintained over time (Fig. 1 D and not depicted). A closer examination of the probe distribution reveals that an enrichment of the normalized signal at the leading edge was noticed in only 4 out of 32 migrating cells. In a large majority of CCL19-stimulated cells (28 out of 32 cells), migration was not accompanied by any detectable translocation of the AKT-PH-CFP probe during a 10-min observation period. (Fig. 1 B and Video 1, available at http://www.jem.org/cgi/content/full/jem.20062079/DC1). Thus, chemokine-dependent PI3K signaling in T cells markedly differs in its intensity from that induced during antigenic stimulation and in various models of cell polarization.

Absence of Rac-dependent amplification of PIP3 synthesis in T lymphocytes

In different cell types, the magnitude of PIP3 production depends on the existence of an amplification system that requires Rac and class IA PI3K. We reasoned that the failure to translocate CFP-AKT-PH in response to chemokines might result from the absence of such an amplification loop in T lymphocytes. To test this hypothesis, we selectively interfered with class IA PI3K signaling by transfecting T cells with the entire p85α regulatory subunit fused to GFP. Indeed, when overexpressed in T cells, the monomer efficiently competes with the activity of endogeneous heterodimeric PI3K triggered by antigen recognition (18). As expected, it also impaired downstream phosphorylation of AKT after anti-CD3 stimulation (Fig. 2 A, middle). In contrast, no effect was observed when CCL19 was used to stimulate T lymphocytes (Fig. 2 A, right). AKT activation in CCL19-stimulated cells was also insensitive to IC87114, a selective inhibitor of the leukocyte-specific p110δ catalytic subunit (Fig. 2 B, right histogram) (19). As a control, TCR-dependent AKT phosphorylation was shown to be completely abrogated by IC87114 (Fig. 2 B, left histogram). WMN, which does not discriminate between class IA and IB PI3K isoforms, inhibited AKT phosphorylation regardless of the stimulus applied to T cells (Fig. 2 B). Because p85α and p110δ are the major regulatory and catalytic class IA subunits in T lymphocytes (20), these results imply that class IA PI3K does not contribute to the PIP3 pool generated by CCL19 stimulation. We also assessed the ability of Rac to directly modulate PI3K activity by overexpressing a constitutively active mutant of this Rho GTPase in T lymphocytes. AKT phosphorylation did not increase above basal levels in T cells transfected with constitutive active RacV12 (Fig. 2 C). In contrast, in NIH-3T3 fibroblasts expressing RacV12, an increase in the level of AKT phosphorylation was observed, consistent with previous reports showing that Rac1 controls normal PIP3-dependent signaling in several cell types (Fig. 2 D) (12, 13). Collectively, our data support the idea that T lymphocytes do not have a 3′-phosphoinositide amplification system coupled to G protein–coupled receptor activation, and that in these cells PI3Kγ alone is responsible for catalyzing the production of this metabolite, which is consistent with previous studies (14, 15).

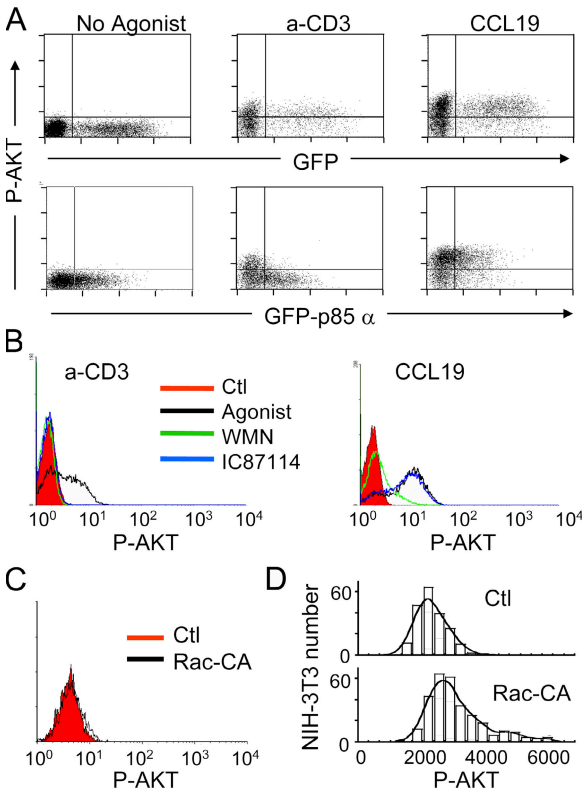

Figure 2. Absence of a Rac- and class Ia PI3K–dependent PIP3 amplification system in T lymphocytes. (A) Human PBT cells transfected with EGFP or EGFP-p85α were left unstimulated or stimulated with either soluble 10 μg/ml anti-CD3 for 15 min or 100 ng/ml CCL19 for 2 min, fixed, stained with anti–P-AKT, and analyzed by flow cytometry. (B) PBT cells were preincubated in the presence of medium alone, 100 nM WMN for 30 min, or IC87114 for 30 min, and were stimulated with either anti-CD3 or CCL19, stained, and analyzed as in A. Results are representative of three independent experiments. The y axis corresponds to the number of T cells. (C) PBT cells were transfected with vector alone or vector encoding a constitutively active (CA) form of Rac. P-AKT was detected by flow cytometry as in Fig. 1 B. The y axis corresponds to the number of T cells. (D) NIH-3T3 fibroblasts were transfected with vector alone or vector encoding a constitutively active (CA) form of Rac. P-AKT was detected on adherent cells by immunofluorescence.

Uncoupling of 3′-phosphoinositide metabolism and actin dynamics

Given the ability of 3′-phosphoinositides to activate Dbl-related GEFs (21), in many cell types PI3K can signal through Rac to initiate actin polymerization. To determine whether a causal link exists between 3′-phosphoinositide metabolism and the assembly of actin polymers in T lymphocytes, we targeted the catalytic subunit p110α to the plasma membrane via a C-terminal CAAX motif (22), thereby rendering PIP3 levels and AKT phosphorylation constitutively high (Fig. 3 A, right). Using the actin content of unstimulated and CCL19-stimulated control cells as a reference interval, we measured the effect of high PIP3 on actin assembly. F-actin levels and cell morphology were indistinguishable in control and p110-CAAX–transfected T lymphocytes (Fig. 3 B and Fig. 3 D, bottom, no agonist), suggesting that PIP3 by itself does not switch on the actin-protrusive machinery in T lymphocytes. This result contrasts with that observed in NIH-3T3 fibroblasts in which the expression of p110-CAAX markedly increases the level of F-actin (Fig. 3 C). Because sites of actin assembly often correlate with local hot spots of PI3K activity (23), we have investigated whether the same correlative distribution could be observed in T lymphocytes. To this end, we evaluated the ability of p110-CAAX–transfected cells to asymmetrically localize F-actin after CCL19 stimulation. If PIP3 had a determinant role in restricting actin assembly to a single site, then uniform PIP3 should result in a matched F-actin distribution. Cotransfection of p110-CAAX and GFP-AKT-PH allowed us to verify that PIP3 was indeed being generated all over the plasma membrane in both quiescent and CCL19-stimulated cells (Fig. 3 D, top). As expected, actin was strongly polarized toward the leading edge of control cells stimulated with CCL19 (Fig. 3 D, bottom). Despite the abundant PIP3 outside the leading edge, p110-CAAX–transfected cells showed asymmetric F-actin and polarized normally (Fig. 3 D, right). Thus, during T cell polarization, PI3K signaling and restriction of actin cytoskeleton dynamics to the leading edge are uncoupled events.

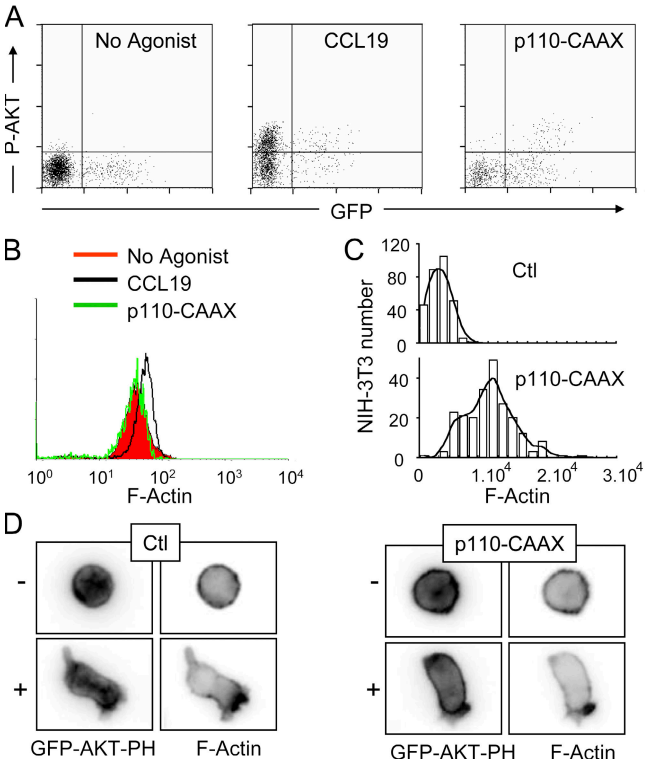

Figure 3. PIP3 does not have an instructive role in F-actin assembly. (A) Human PBT cells were cotransfected with EGFP and either empty vector or p110-CAAX. P-AKT levels in GFP-positive cells were detected by flow cytometry. Empty vector-transfected cells were stimulated with 100 ng/ml CCL19 for 2 min to compare the magnitude of P-AKT induced by physiological activation with that induced by the expression of p110-CAAX. (B) The same conditions as in A were used, except that TRITC-conjugated phalloidin was used to stain F-actin. Data are representative of three independent experiments. The y axis corresponds to the number of T cells. (C) NIH-3T3 fibroblasts were transfected with vector alone or vector encoding p110-CAAX. F-actin was detected on adherent cells by immunofluorescence. (D) PBT cells cotransfected with EGFP-AKT-PH and either empty vector (Ctl) or p110-CAAX were left unstimulated (−) or stimulated (+) in suspension with 100 ng/ml CCL19 for 2 min, fixed, and stained with Texas red–conjugated phalloidin. Images show one representative cell for each condition.

PI3K activity is not essential for T cell polarization in vitro

We analyzed the effect of PI3K inhibition on the morphologic changes triggered by CCL19. As shown in Fig. 4 A, inhibition of PI3K by WMN does not interfere with T cell

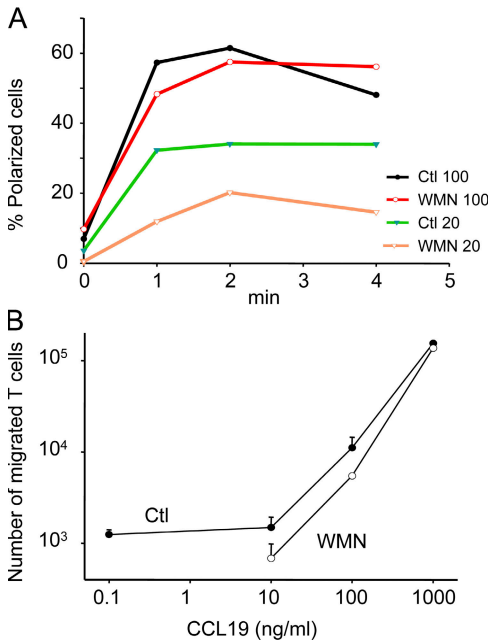

Figure 4. PI3K Activity is not essential for T cell polarization or migration in vitro. (A) PBT cells preincubated with 100 nM WMN for 30 min or medium alone were stimulated with CCL19 (20 and 100 ng/ml), and cell polarization was video recorded for 4 min. Quantification of one representative experiment is shown. (B) Transwell assay performed with control (Ctl) or WMN-treated PBTs. Data are representative of three experiments, and error bars represent the SD of duplicate samples.

polarization triggered by a large concentration (100 ng/ml) of CCL19. However, a twofold reduction in the number of WMN-treated polarized cells was observed when T cells were stimulated with a low concentration (20 ng/ml) of CCL19. Similarly, WMN-treated T cells demonstrated a reduced transwell migration mostly at low concentrations of CCL19 but not at the highest concentrations of CCL19 (Fig. 4 B), confirming previous results (14, 15). The unusual involvement of PI3K in chemokine-induced T cell polarization and migration studied in vitro prompted us to investigate the importance of this signaling pathway on T cell motility measured in a native environment.

LN slices: a new system to study T cell motility in a physiological environment

To study T cell motility in a physiological environment, we have developed an excised LN slice preparation adapted from the recently described preparation of thymic slices (24). In brief, LNs embedded in low-melting temperature agarose were sliced into 320-μm thick sections. A mixture of T lymphocytes and B lymphocytes labeled with two different fluorescent dyes was overlaid on the slice surface and allowed to migrate within the slice. After 1 h of incubation, the cells that remained at the slice surface were washed, and the preparation was turned upside down and observed with a plain fluorescence inverted microscope that allowed us to visualize cells at depths up to 40 μm within the slice. Under these conditions, we found that both categories of lymphocytes had migrated into the slice and positioned in their respective T cell and B cell zones (Fig. 5 A). In particular, T cells were excluded from B cell zones (Fig. 5 B). We then analyzed the behavior of recruited T cells in the outer cortical region beneath the B cell zone by acquiring, for 20-min periods, stacks of images from the cut surface to 50 μm in depth (Fig. 5 C). Most T cells were highly motile (Fig. 5D and Video 2, available at http://www.jem.org/cgi/content/full/jem.20062079/DC1), with a mean velocity of 7.5 μm/min. Analysis of cell trajectories indicated that T cells randomly migrated within the node, a finding consistent with that previously reported in intact LNs (Fig. 5 E). After adoptive transfer of fluorescent T cells, larger mean velocities and motility coefficients were obtained (Fig. S1) because of the larger number of stationary cells observed in the overlay method. This may reflect the fact that cells made unhealthy by ex vivo manipulations (purification and labeling) may enter the slice but, after adoptive transfer, do not cross the HEV barrier. Consistent with this interpretation, stationary cells were found in the superficial region of the slice in the overlay condition (Fig. S1 B) but not after adoptive transfer (Fig. S1 D), When cells positioned within the first 10 μm from the cut surface of the slice were excluded from the analysis, we obtained a mean velocity >10 μm/min after both the adoptive transfer experiment and the T cell overlay. These results demonstrate that the ex vivo LN slice preparation preserves the native three-dimensional environment that induces T cell motility.

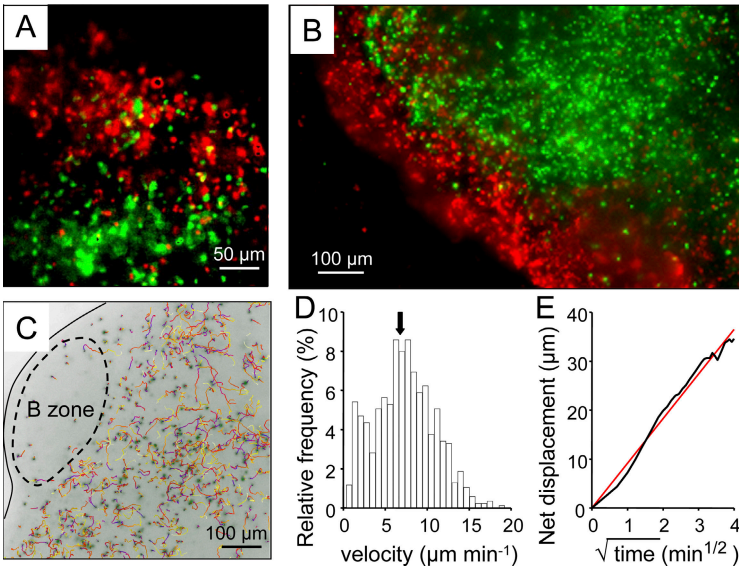

Figure 5. T cells are highly motile within LN slices. (A) Fluorescently labeled T cells (CMFDA; green) and B cells (fura-2; red) were added to a LN slice 1 h before the recording. This image is the maximum projection of four images spanning 40 μm in the z direction beneath the cut surface of the slice. (B) Fluorescent T cells (CMFDA; green) were added to the LN slice. Resident B cells were subsequently labeled with a B-specific antibody (B220; red). The image was captured as in A. (C) Individual trajectories of T cells in the outer paracortex region of a LN slice depicted in x–y views during a 20-min recording. Tracks are color coded to indicate time progression from the beginning (blue) to the end (yellow) of imaging. The black line follows the edge of the node, whereas the dashed oval delimits the B cell zone. Video 2 represents time-lapse animation of these cells. (D) T cell velocity profile within a LN slice whose tracks are represented in C. The average speed is indicated with an arrow. (E) The linear relation between net displacement (average of 850 cells whose tracks are represented in C) and square root of time is compatible with random individual displacements. Video 2 is available at http://www.jem.org/cgi/content/full/jem.20062079/DC1.

In LN slices, migrating T cells display transient Ca^{2+} increases

We took advantage of the fast penetration of overlaid T cells into the slice to measure their intracellular Ca^{2+} concentration with the fluorescent dye fura-2. Occasional Ca^{2+} increases (Fig. 6 A) in the absence of exogenously added antigen were observed in approximately one quarter of migrating cells during 10-min observation periods (Video 3, available at http://www.jem.org/cgi/content/full/jem.20062079/DC1). As shown in Fig. 6 B, these transient responses occurred more frequently when the cells were arrested, consistent with previous observations suggesting that Ca^{2+} elevations induced cell immobilization (24, 25). The percentage of Ca^{2+}-responding cells in the outer paracortex was similar to that measured deeper in the T zone (Fig. 6 C).

Proper T cell localization and motility within the LNs is Gαi dependent

We next investigated the nature of the molecules responsible for T cell recruitment and movements in the LN environment. As an initial approach, we used pertussis toxin (PTX), which ADP ribosylates and inactivates the αi subunit of the heterotrimeric G proteins used by most chemokine receptors to transmit their intracellular signals. As a control, we used T cells treated with suB, the B subunit of PTX, which binds to the cell surface but does not possess catalytic activity. The penetration of PTX-treated and control T cells loaded with two different fluorescent dyes was simultaneously observed. When T cells were incubated for 2 h with PTX, the fraction of cells that migrated in the slice was considerably lower than that of control T cells (Fig. 7 A and Fig. 8 A). Thus, T cell recruitment and proper positioning within the slice is PTX sensitive and, therefore, very likely chemokine dependent, although one cannot exclude the participation of other Gαi-dependent factors.

We next examined the importance of Gαi signaling on T cell motility in the three-dimensional LN environment. The previous PTX protocol could not be used because of the paucity of PTX-treated T cells inside the slice. We thus used a modified protocol aiming to inactivate Gαi only after T cells had been properly recruited and positioned. It has been reported that PTX inhibition of Gαi is not instantaneous

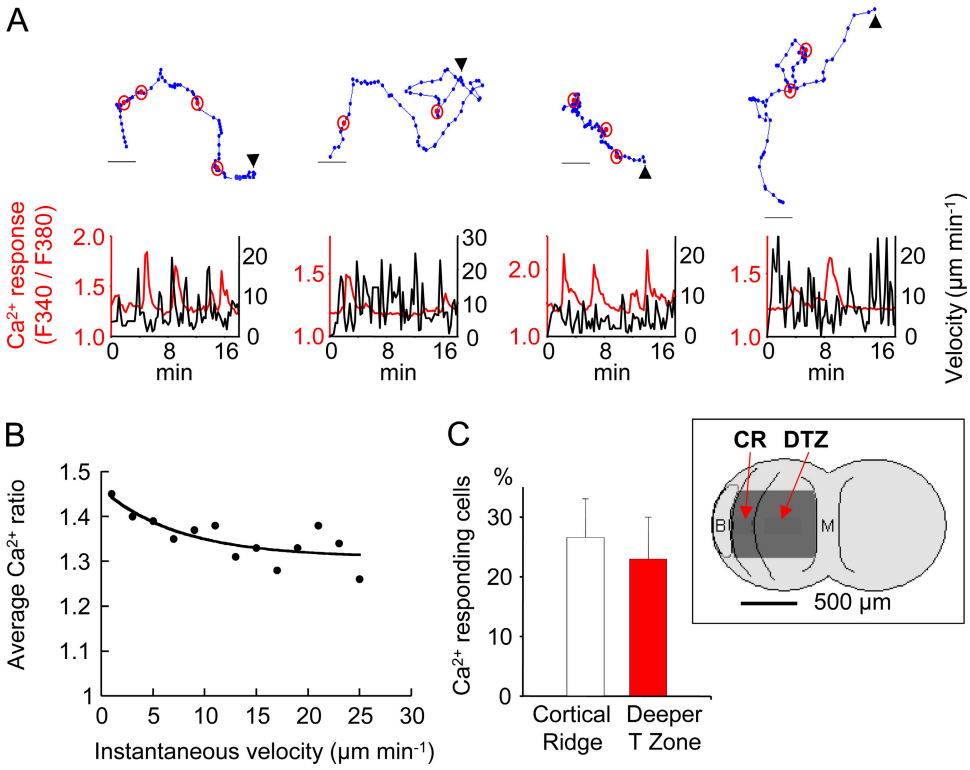

Figure 6. T cells display antigen-independent Ca^{2+} increases within LN slices. (A) Ca^{2+} responses and motility in four representative T cells within a LN slice. T cells were loaded with fura-2 and added to a LN slice 30 min before the recording. (top) The sequential positions of migrating T cells (blue dots) at successive 20-s intervals. Ca^{2+} spikes are indicated by circled red dots. Bar, 10 μm. (bottom) The simultaneous measurement of Ca^{2+} level (red) and instantaneous (black) velocities plotted against time for the above tracked cells. Arrowheads indicate where a track starts. A time-lapse animation of the leftmost cell is shown in Video 3. (B)Relation between instantaneous velocity and Ca^{2+} levels. Dots are average Ca^{2+} values corresponding to velocities binned every 2 μm min^{-1}. Data are from 11 cells. (C) Percentage of Ca^{2+}-responding cells measured in two distinct areas of the LN slice, the cortical ridge (CR) and the deeper T zone (DTZ). Data are the means ± SD from four independent experiments in which >50 cells were analyzed per experiment. The inset schematizes the positions, in a LN, of the CR and the DTZ in relation to a B follicle (B) and the medulla (M). Video 3 is available at http://www.jem.org/cgi/content/full/jem.20062079/DC1.

but takes place after a delay of at least 1 h (26). We more precisely evaluated this delay by performing in vitro experiments in which T cells were incubated for 10 min with PTX, washed, and stimulated with CCL19 at various times after the toxin treatment. No inhibition was evident 1 h after PTX treatment, but after 2.5 h an almost complete inhibition of CCL19-induced T cell polarization was observed (Fig. S2, available at http://www.jem.org/cgi/content/full/jem.20062079/DC1).

T cells were thus incubated with PTX or suB for 10 min, washed, labeled with two different fluorescent dyes, and overlaid onto a LN slice. 3 h later, the motility of both cell types was measured in the slice. Both the velocity and the motility coefficient of PTX-treated T cells were markedly lower than those of suB-treated lymphocytes (Fig. 7, C and D). In the presence of PTX, a majority of cells remained quasi-stationary. Representative examples of such PTX-dependent decreases in T cell motility are shown in Fig. 7 B and Video 4 (available at http://www.jem.org/cgi/content/full/jem.20062079/DC1). A similar finding was observed if T cells were treated for 10 min with PTX, were adoptively transferred by i.v. injection, the LNs excised and sliced 3 h later, and the motility of adoptively transferred T cells measured immediately in the LN slice (unpublished data). These results indicate that Gαi signaling is required for the motility of T lymphocytes within the LN slice.

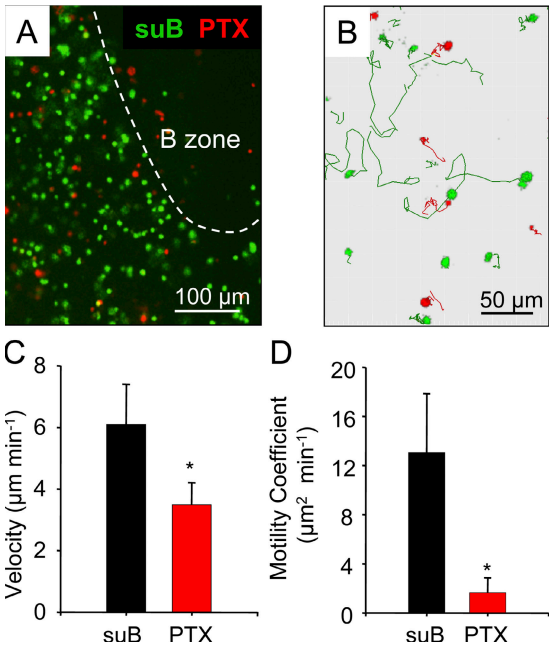

Figure 7. T cell recruitment and migration within LN slices are inhibitable by PTX. (A) Image of control T cells treated with the inactive B subunit of PTX (green) and PTX-treated T cells (red) in a LN slice. T cells were incubated for 2 h with 100 ng/ml suB or PTX, respectively labeled with CMFDA or fura-2 and overlaid on a LN slice. The dashed line delimits the B cell zone. (B) Tracks of individual suB-treated (green) and PTX-treated (red) T cells from one slice over a period of 20 min. Video 4 represents time-lapse animation of these cells. (C and D) Velocities and motility coefficients of suB- and PTX-treated T cells within LN slices. T cells were incubated for 10 min with 100 ng/ml suB or PTX, washed, labeled with two different fluorescent dyes, and overlaid on a LN slice. T cell behavior was analyzed 3 h after the initial toxin treatment. Results in C and D represent the mean and SD calculated from six independent experiments in which >100 cells were analyzed per experiment. *, $P < 0.05$. Video 4 is available at http://www.jem.org/cgi/content/full/jem.20062079/DC1.

CCR7 and its ligands regulate T cell recruitment and migration within LN slices

We next sought to determine the nature of the chemokines involved in T cell trafficking within LN slices. To examine the role of CCR7 ligands, fluorescently labeled T cells were added to LN slices of *plt* mice that lack lymphoid CCL19 and CCL21 chemokines. The number of T cells that had migrated into LN slices of *plt* mice was reduced to ∼40% compared with that seen in control, WT slices (Fig. 8 A). To better delineate the importance of CCL19 and CCL21 in T cell recruitment and positioning within the slice, we used T cells from CCR7-deficient mice. When WT and CCR7-deficient cells labeled with two different dyes were overlaid onto a WT slice, we observed after 1 h of incubation that the vast majority of CCR7-deficient T cells were mislocalized and scarce in the T cell zone but accumulated in the subcapsular region of the LNs, attesting to the presence, in these areas, of chemoattractants other than CCL19 and CCL21 (Fig. 8 B and Video 5, available at http://www.jem.org/cgi/content/full/jem.20062079/DC1). We checked that the recruited cells in the absence of CCR7 or its ligands were representative of the starting population and not biased toward memory of effector T cells, which express high levels of CD44. As shown in Fig. S3 A, the fraction of $CD44^{hi}$ T cells that had entered slices of *plt* mice was similar to that measured before plating the cells. Similar results have been obtained with CCR7-deficient T cells recruited into WT slices (Fig. S3 B).

To assess the role of CXCL12, we used AMD3100, a selective antagonist of CXCR4 (27). We initially checked that T cell polarization triggered by CXCL12 in vitro was efficiently blocked by AMD3100 (unpublished data). Control and AMD3100-treated T cells were then overlaid onto LN slices of control and *plt* mice. As shown in Fig. 8 A, the CXCR4 antagonist did not reduce the recruitment of T cells into slices from WT mice. However, in the absence of lymphoid CCL19 and CCL21, the CXCR4 antagonist further reduced T cell recruitment to a level almost similar to that observed when T cells were treated with PTX. These experiments reveal the presence within the node of CCR7 ligands and CXCL12 that together contribute to attract overlaid T cells into the tissue.

We next assessed the importance of CCR7 and its ligands on the T cell motility measured in the outer cortical region of the slice. As shown in Fig. 8 (C–F) and Video 5, the velocity and motility coefficients of T lymphocytes in the absence of CCR7 or its ligands were markedly reduced compared

with those measured in WT slices. We used the CXCR4 antagonist to investigate the participation of CXCL12 in T cell motility within the LN slice. Untreated T cells were overlaid onto a LN slice that was subsequently incubated with AMD3100 1 h before and during the imaging procedure. In a WT slice, AMD3100 did not affect T cell motility (not depicted) and, importantly, did not further reduce velocities and motility coefficients measured in the absence of CCR7 or its ligands (Fig. 8, C–F). The absence of a CXCR4-dependent motility was confirmed with another CXCR4 antagonist, an N-terminally truncated (5-67) CXCL12 (28) (unpublished data). These data suggest that T cell motility within the LN slice is CXCL12 independent.

As it has recently been shown that T cells within the LNs migrate almost exclusively along FRC networks (7), we examined the precise distribution of CCL21 and CXCL12 within the T zone of LN slices. As shown in Fig. S4 A (available at http://www.jem.org/cgi/content/full/jem.20062079/DC1), CCL21 is expressed in the T zone as well as the medulla. In addition, CCL21 staining presents a striking overlap with that of ER-TR7, consistent with previous data (Fig. S4 B) (29–32). In contrast and as previously shown (33), CXCL12 was enriched in the medulla and subcapsular regions but poorly expressed in the T area (Fig. S4, C and D). Importantly, the weak CXCL12 signal in the T zone was not associated with the FRC network (Fig. S4 D). In addition, no staining of CCL19 was observed in LN slices. All of these data sustain the idea that CCL21 closely associated with FRCs provides an important chemokinetic signal to T cells.

PI3K does not control T cell motility measured within LN slice

Having shown the importance of chemokines in T cell motility within LN slices, we assessed the role played by PI3K on this response. The behavior of differently labeled control and WMN-treated T cells was simultaneously observed in the same LN slice 1 h after their addition to the preparation. T cells correctly localized to the T cell zone of the LNs irrespective of the treatment administered before the transfer. However, the number of WMN-treated cells recruited in the slice was lower than that of control cells (Fig. 9 A). Importantly, no differences were found in the velocities and motility coefficients of coplated control and WMN-treated cells in the T cell zone (Fig. 9, A–C and Video 6, available at http://www.jem.org/cgi/content/full/jem.20062079/DC1). To confirm these results, adoptive transfer experiments were performed with control and WMN-treated cells. 2 h after the transfer, we observed that WMN-treated cells were not homogeneously distributed compared with control cells (Fig. 9 D and Video 7). Hence, a fraction of WMN-treated cells accumulated in restricted areas that were identified, with

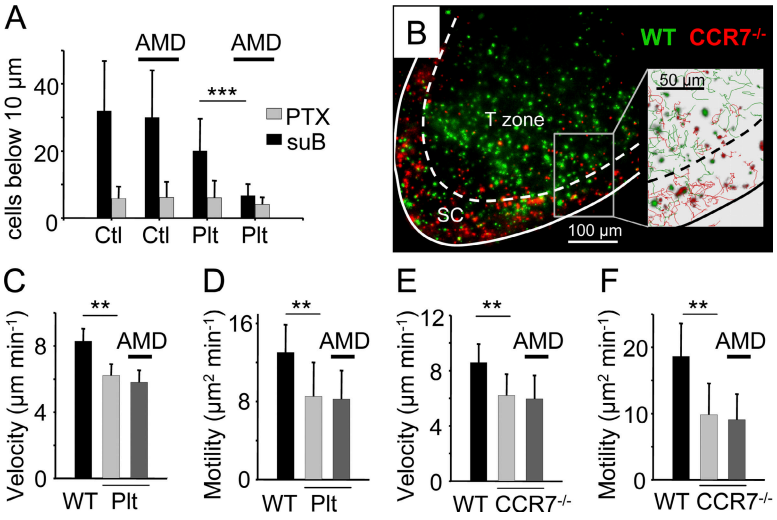

Figure 8. T cell motility within the LN slice depends on the CCR7 ligands. (A) Quantification of cells found 10 µm below the surface of the slice in a 50-µm^2 zone. Cells were automatically counted in three dimensions with Imaris software. Cells were treated for 2 h with 100 ng/ml suB or PTX, washed, labeled with fluorescent dyes, and overlaid on a LN slice of WT and *plt* mice. Slices were treated or not with 5 µg/ml AMD3100 that selectively inhibits the CXCL12–CXCR4 interaction. Data give the mean of three experiments ± SD. (B) Fluorescently labeled T cells (CMFDA; green) and CCR7-deficient T cells (fura-2; red) were added to a LN slice 1 h before the recording. In the zoomed image (inset) of the outlined region, tracks of WT (green) and CCR7-deficient (red) T cells are represented over a period of 20 min. The dashed line delimits the subcapsular sinus (SC) region from the T cell zone. The white line indicates the edge of the LN. Video 5 represents time-lapse animation of these cells. (C and D) Velocities and motility coefficients of T cells that have been overlaid on WT or *plt* slices. Where indicated, slices were treated with 10 µg/ml AMD3100 during the recording. (E and F) Velocities and motility coefficients of WT and CCR7-deficient T cells that have been overlaid on WT slices 1 h before the recording. Slices were treated where indicated with AMD3100 as in C and D. Shown are means ± SD of at least five independent experiments in which >100 cells were analyzed per experiment. **, $P < 0.01$; ***, $P < 0.001$. Video 5 is available at http://www.jem.org/cgi/content/full/jem.20062079/DC1.

peripheral node addressin labeling, as HEVs (Fig. S5), as if PI3K inhibition slowed down their entry in the LNs as previously suggested (15). Despite this, a substantial proportion of WMN-treated T cells could be found together with control cells in the T cell zone. Because WMN-treated T cells accumulated in HEVs exhibited a reduced motility, it was important to analyze T cell behavior outside of these areas. Our data indicate that the velocity of adoptively transferred T cells that had reached the T cell zone was not affected by PI3K inhibition (Fig. 9, E and F), as already observed when T cells were added directly to the slice. Of note, PI3K activity in transferred T cells was still inhibited by WMN 2 h after their injection, because phosphorylation of AKT after CCL19 stimulation was abolished (unpublished data). Thus, basal T cell motility within peripheral LNs is essentially independent of PI3K signaling.

DISCUSSION

The cellular and molecular basis of T cell migration within LNs, a key step in the initiation of adaptive immune responses, is far from being well understood. In this paper, we have analyzed a set of mechanisms governing T cell mobility in vitro and in a three-dimensional LN structure. Our results show that intranodal T cell trafficking depends on several chemokines and, in particular, on CCR7 and its ligands. PI3K plays a minor role in T cell polarization and motility studied in vitro and in an intact three-dimensional nodal structure.

Even though there is longstanding evidence that PI3K orchestrates the polarized responses to chemoattractants in a variety of cells (11), lymphocytes seem to behave in a special way (34). In vivo homing assays have recently shown that PI3K does not markedly contribute to lymphocyte migration to peripheral LNs (15), suggesting that other PI3K- independent routes prevail in lymphocytes.

Our findings corroborate and extend these observations, because neither lymphocyte polarization in response to homeostatic chemokines nor the migration patterns within LN slices were notably impaired by WMN. Consistent with this conclusion, we did not find a causal link between the levels and spatial distribution of 3′-phosphoinositides and the extent or site of actin polymerization. This is in marked contrast with other motile cells in which the link between actin dynamics and PI3K is well established (35–37). The critical parameter defining whether PI3K might effectively couple to downstream actin remodeling pathways is likely to be the set of Rac GEFs expressed in the cell. Rac activity in chemokine-activated lymphocytes is mostly controlled by DOCK2 (38, 39), which is not activated in a PI3K-dependent

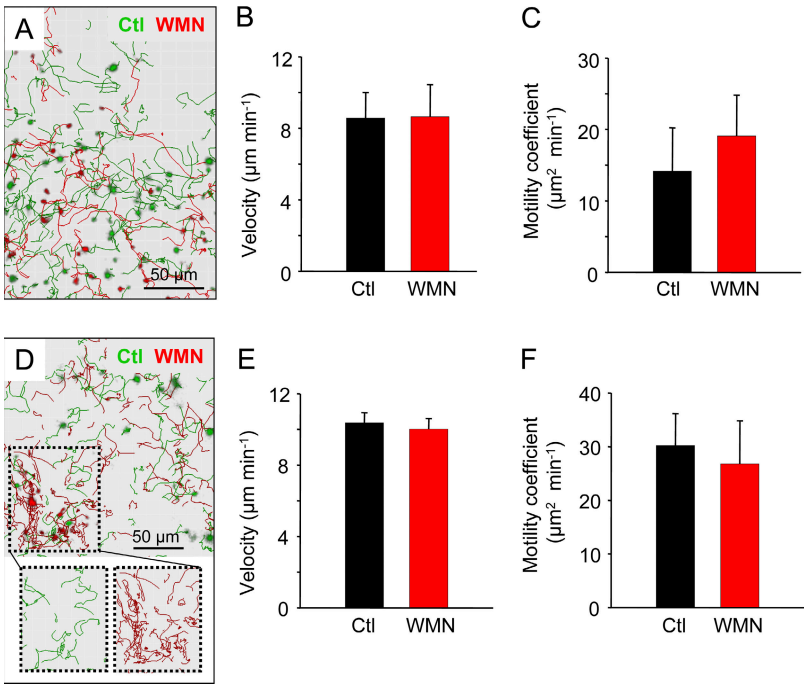

Figure 9. PI3K Activity is not essential for T cell motility within LN slices. T cells were incubated with 100 nM WMN for 30 min and labeled with CMFDA (red), whereas control (Ctl) cells were labeled with fura-2 (green). Cells were overlaid on a LN slice (A, B, and C) or adoptively transferred (D, E, and F). 1 h after cell plating or 2 h after adoptive transfer, T cell motility was analyzed in the T zones of LN slices. (A and D) Tracks of individual Ctl and WMN-treated cells added to a slice (A) or after adoptive transfer (D) during a 20-min recording. The outlined region in D shows the accumulation of WMN-treated T cells in restricted areas of the LN slice after adoptive transfer. Videos 6 and 7 represent time-lapse animations of cells in A and D, respectively. (B, C, E, and F) Velocities and motility coefficients of Ctl and WMN-treated cells added to a slice (B and C) or after adoptive transfer (E and F). Data are the means ± SD of at least five independent experiments in which >100 cells were analyzed per experiment. Videos 6 and 7 are available at http://www.jem.org/cgi/content/full/jem.20062079/DC1.

way (15, 40). Thus, it is possible that the developmental acquisition of DOCK2 during lymphopoiesis might selectively uncouple PI3K from the actin cytoskeleton regulatory networks in the lymphoid lineage, whereas myeloid leukocytes, which do not express DOCK2, preserve this otherwise conserved link.

Our observations underscore other important differences between these two lineages. The metabolism of 3′-phosphoinositides in lymphocytes is not wired to an amplification mechanism, as previously described in neutrophils and *Dictyostelium*. In these cells, the production of PIP3 has an autocatalytic component that depends on the dual positioning of Rac both downstream of PIP3 and upstream of PI3K (13, 35, 41, 42). A key point in this positive feedback loop is the ability of Rac to recruit class IA PI3K isoenzymes that amplify the initial PI3Kγ-dependent wave of PIP3 (12, 13). In this paper, we show that neither Rac nor class IA PI3K contribute to the PIP3-dependent activation of AKT, suggesting that the PIP3 pool is exclusively maintained by the activity of PI3Kγ, which is consistent with earlier studies (14, 15).

Several lines of evidence indicate that the synthesis of PIP3 in lymphocytes might be rapidly counterbalanced by the reverse 3′-phosphatase–catalyzed reaction. Consistent with this, the lipid phosphatase PTEN was found uniformly distributed along the anterior–posterior axis of the cell, implying an extensive colocalization with the 3′-kinase activity during lymphocyte polarization (unpublished data). Thus, the lack of a signal amplification system, combined with the mutual antagonism between PI3K and PTEN, seems to contribute to maintaining the relatively low 3′-phosphoinositide levels at the plasma membrane. However, one cannot exclude the existence, upon chemokine stimulation, of a very early, undetected, and transient PIP3 increase sufficient to induce the membrane recruitment of AKT, followed by its phosphorylation. In vitro experiments show that PI3K is considerably involved in chemokine-induced T cell polarization only at chemokine concentrations leading to submaximal responses. Whether this suboptimal stimulation might be mimicked in a physiological environment relevant to T cell biology is not known.

To further study the importance of PI3K and of chemokines in T cell polarization, motility, and migration, we have developed a new experimental system of thin slices of LNs, adapted from the thymic slices recently described (24). LN slices constitute an experimental system that offers a series of interesting properties. First, observations can be made with a plain fluorescence microscope. The spatial resolution achieved with this system is not as good as with a confocal or a two-photon microscope, but it has the advantages of simplicity, a lower cost, and a larger choice of excitation wavelengths. Second, we have shown that lymphocytes added to the slice rapidly reach their appropriate location (<1 h) as a result of an active chemokine-dependent recruitment leading to an accurate lymphocyte positioning. We took advantage of this fast recruitment to monitor the Ca^{2+} level of migrating T cells within the slice. Indeed, fluorescent Ca^{2+} dyes have a tendency to leak out of the cells over time, which limits their use after adoptive transfer experiments. In this study, we show that a substantial proportion of T cells migrating within the slice display small and transient Ca^{2+} responses similar to those observed in vitro when T cells interact with DCs (43). A third advantage of this experimental system is that T cells move within the LN structure without having to walk through the HEV barrier. One may thus separately analyze the control of T cell entry into the LNs, as well as that of its motility after crossing the HEV barrier. In addition, the accessibility of the culture system allows one to acutely interfere with the molecular control of cell migration.

This novel preparation presents some limitations that deserve to be discussed. First, after T cell overlay, stationary cells were observed in the superficial region of the slice. The presence of these cells lowers the average motility and could complicate the interpretation of some of the experiments. However, all the key results obtained in the slice preparation after cell overlay have been confirmed by adoptive transfer experiments in which the T cell motility is very similar to that observed in intact LNs.

Second, one may be concerned by the fact that tissue damage associated with the slicing may affect T cell behavior. Such an issue is generally not raised against the study of neuronal networks in brain slices, and although we have no indication that our data were affected by such damages, this potential problem must be kept in mind.

Finally, phototoxicity is in principle more severe with one-photon microscopy than with two-photon microscopy. Again, we observed no sign of overt phototoxicity, but it is likely that a LN slice preparation combined with two-photon imaging will increase the spatial resolution and reduce the phototoxicity.

We have shown that the apparently random migration of T cells in LNs does not reflect a spontaneous behavior of T cells but is a response to intranodal chemokines exerting a chemokinetic effect there, with CCR7 ligands playing a key role in this process. In addition, CCL21 is expressed along FRCs present in the T cell zone (Fig. S4) (29–32). These and other results (7) demonstrate the crucial role of FRCs in providing both a support and a chemokinetic trigger to T cells.

Besides CCR7 ligands, CXCL12 was a reasonable candidate for the regulation of intranodal T cell motility. Indeed, CXCR4 is expressed by naive T cells, and our data show that this chemokine is expressed in the LNs (see also reference 33) and regulates the recruitment of overlaid T cells in the tissue in the absence of CCR7 or its ligands. Unexpectedly, two specific and potent CXCR4 antagonists applied to the LN slice after T cells have been recruited did not affect T cell motility, even in the absence of CCR7 or its ligands. We propose that T cell recruitment in the slice is a function not only of T cell motility but also of chemokine gradients. The regulation of these two parameters (chemokinesis and chemotaxis) is not necessarily unique. At the surface of the slice, T cells not yet adherent to FRCs would be under the

influence of different chemokine gradients (mainly CCL19/CCL21 and CXCL12). On the other hand, T cell motility in the nodal structure would depend on CCR7 and at least one other receptor, but not on CXCR4. This would be consistent with the observed CCR7-dependent effects on T cell motility, on the colocalization of CCL21 but not CXCL12 with ER-TR7, and on the fact that we have evidenced a CCR7-independent component of T cell motility. In the future, it will be of major interest to identify the molecules that contribute to regulating intranodal T cell motility, together with CCR7 ligands.

In conclusion, the LN preparation in this study that was used for the first time has allowed us to demonstrate that T cell motility within LNs is not an intrinsic property of T lymphocytes but is driven in a PI3K-independent manner by the lymphoid chemokine-rich environment.

MATERIALS AND METHODS

Human T Cells. Human PBMCs were obtained from the whole blood of healthy human donors in agreement with Etablissement Français du Sang guidelines. Peripheral blood T cells (PBT cells) were purified from PBMCs by negative selection using a T cell isolation kit (BD Biosciences).

Transfection. Human PBT cells were transfected using Nucleofection technology (Amaxa), according to the manufacturer's instructions, and were used 18 h after transfection. NIH-3T3 fibroblasts cultured on glass coverslips were transfected with Lipofectamine Plus (Invitrogen) and used 15 h after transfection.

Plasmids and inhibitors. The CFP-AKT-PH and GFP-p85 constructs have been previously described (18). P110-CAAX was provided by P. Parker (London Research Institute, London, UK) (22). pEGFP-C3 and pYFP-C3 (CLONTECH Laboratories, Inc.) were used as controls. 100 nM WMN (Calbiochem) and 5 μM IC87114 (provided by D. Bouscary, Institut Cochin, Paris, France) were used.

Intracellular staining for flow cytometry. Human PBT cells were stimulated in suspension with CCL19 (PeproTech) or anti-CD3 (UCHT1; BD Biosciences), fixed for 10 min with 4% paraformaldehyde at 37°C, and permeabilized with 0.1% saponin. TRITC-conjugated phalloidin (Sigma-Aldrich) and anti–P-AKT (Ser 473; Cell Signaling Technology) were used for intracellular staining. For secondary detection, biotin-conjugated anti–rabbit antibodies (Jackson ImmunoResearch Laboratories) and streptavidin-phycoerythrin (BD Biosciences) were used.

Immunofluorescence. Human PBT cells were stimulated in suspension with CCL19 (PeproTech), fixed with 4% paraformaldehyde, permeabilized for 10 min with 0.2% Triton X-100, and stained with Texas red–conjugated phalloidin (Invitrogen). Stained cells were deposited onto microscope slides, mounted in reagent (FluorSave; Calbiochem), and visualized with an inverted microscope (Eclipse TE2000-E; Nikon) equipped with either 40× or 60× oil objectives (Plan Apo; Nikon) and MetaVue imaging software (Universal Imaging). Adherent NIH-3T3 cells were processed as T cells. Fluorescence intensity of F-actin and P-AKT was measured on adherent fibroblasts and quantified using the integrated morphometric analysis function of MetaMorph software (Universal Imaging).

Time-lapse imaging. For live cell migration experiments, glass coverslips were coated overnight at 4°C with 3 μg/ml human ICAM-1–Fc (R&D Systems), washed with PBS, and blocked with PBS containing 1% BSA for 30 min at 37°C. T cells were plated on the ICAM-1 layer and stimulated with recombinant CCL19 (PeproTech). Image acquisition was done on an inverted microscope equipped with a 60× objective and MetaFluor imaging software. Images were acquired every 3 s. In some experiments, cell polarization was assayed in suspended T cells.

PIP3 localization. T cells were cotransfected with CFP-AKT-PH and YFP, a cytosolic marker. PIP3 distribution was quantified from the normalized ratio images of CFP-AKT-PH to YFP, as previously described (23). A translocation index was calculated as the ratio of the normalized ratios (CFP/YFP) measured at the cell periphery and in the center of the cells. The contour of the cell was automatically defined with MetaMorph software.

Mice. CCR7-deficient mice on a C57BL/6 background were obtained from M. Lipp (Max-Delbrück-Center for Molecular Medicine, Berlin, Germany). BALB/c-plt/plt mice were provided by H. Nakano (Duke University Medical Center, Durham, NC). WT C57BL/6 and BALB/c mice were purchased from the Jackson Laboratory. Experiments were performed in accordance with the guidelines of the French Veterinary Department.

Cells and LN slices. LN slice preparation was adapted from the recently described preparation of thymic slices (24). In brief, inguinal, axillary, and brachial mouse LNs were initially embedded in 4% low-gelling-temperature agarose (type VII-A; Sigma-Aldrich) prepared in PBS. 320-μm slices were cut with a vibratome (VT 1000S; Leica) in a bath of ice-cold PBS. Slices were submerged in RPMI 1640 plus 10% FCS at 4°C for a few minutes and were transferred to 0.4-μm organotypic culture inserts (Millicell; Millipore) in 35-mm Petri dishes containing 1 ml RPMI 1640 plus 10% FCS in an incubator at 37°C/6% CO_2.

T cell and B cell suspensions were obtained from peripheral and mesenteric LNs. T cells from CCR7-deficient mice were obtained from spleens. Cells were purified by negative selection (Miltenyi Biotec). Lymphocytes were incubated for 5 min at 37°C with 1 μM 5-chloromethylfluorescein diacetate (CMFDA; Invitrogen) or 45 min at 37°C with 2 μM fura-2 AM (Invitrogen) in HBSS. Cells were washed in RPMI 1640 plus 10% FCS and resuspended in this medium. In some experiments, T cells were pretreated with 100 ng/ml PTX or the B subunit of the toxin (Calbiochem) for the times indicated in the figures at 37°C and washed twice in RPMI 1640 plus 10% FCS. T cells were sometimes incubated for 30 min with 100 nM WMN. According to the experiments, between 10^5 and 5×10^5 lymphocytes in 10–20 μl of RPMI 1640 plus 10% FCS were plated onto the cut surface of each slice. To concentrate the cells on the tissue, a stainless steel ring was placed on the agarose surrounding the slice. To inhibit the CXCL12–CXCR4 interaction, T cells were plated onto LN slices with 5 μg/ml AMD3100 (27, 44), a specific and potent CXCR4 antagonist obtained from the National Institutes of Health AIDS Research and Reference Reagent Program. Slices were incubated for 1 h at 37°C/6% CO_2, gently washed to remove the residual cells that had not penetrated the tissue, and kept in the incubator before the imaging experiment. To investigate the role of CXCR4 on T cell motility within LN slices, untreated T cells were initially allowed to enter the slice for 20 min. Slices were treated with 10 μg/ml AMD3100 for 1 h in the incubator and superfused with 5 μg/ml AMD3100 during the recording. In some experiments, 1 μM of an N-terminally truncated (5-67) CXCL12 provided by F. Bachelerie (Institut Pasteur, Paris, France) was used as another CXCR4 antagonist.

Adoptive transfer. $5–10 \times 10^6$ fluorescently labeled cells/mouse were injected into the retroorbital vein. In some experiments, T cells were pretreated before the injection with 100 ng/ml PTX, the B subunit of the toxin, or with 100 nM WMN at 37°C for the times indicated in the figures. 1–3 h later, LNs were excised and processed for sectioning as described in the previous paragraph.

Video imaging of T cell behavior within LN slices. Imaging experiments were performed with an inverted microscope equipped with a chamber thermostated at 37°C. The preparation was placed upside down on nylon threads glued to each of the extremities of a glass coverslip. In these conditions, the slice lies a few microns above the bottom of the dish, which

facilitates renewal of the perfusion solution bubbled with 95% O_2 and 5% CO_2. The preparation was perfused at a rate of 1 ml/min with bicarbonate buffered solution (130 mM NaCl, 2.5 mM KCl, 1.3 mM NaH_2PO_4, 26 mM $NaHCO_3$, 1 mM $MgCl_2$, 2 mM $CaCl_2$, and 10 mM glucose, pH 7.4, when equilibrated with a mixture of 95% O_2 and 5% CO_2). T cell behavior within a LN slice was analyzed in the T cell area.

For four-dimensional analysis of cell migration, stacks of four sections (z step = 13.3 μm) were acquired with MetaView software (Universal Imaging) every 30 s for 20 min, at depths up to 40 μm. Cell motility was analyzed with Imaris software (version 5.1; Bitplane). Videos were made by compressing the z information into a single plane with the best focus function of MetaMorph.

Ca^{2+} measurements within LN slices. Fura-2 AM–loaded T cells were alternatively excited at 350 and 380 nm. A single section located 20–30 μm from the surface of the slice was acquired every 20 s. Emissions at 510 nm were used for the analysis of Ca^{2+} responses with MetaFluor software. Ca^{2+} values were represented as a ratio: fluorescence intensity at 350 nm/flurorescence intensity at 380 nm. T cells were considered responsive when the amplitude of their responses reached at least twice that of the background.

Immunohistochemistry. Slices were stained with the following antibodies: anti-CD45R B220 (RA3-6B2; Cedarlane), anti–peripheral node addressin (MECA-79; BD Biosciences), anti–ER-TR7 (ER-TR7; BMA Biomedicals). After 45 min of staining with the primary antibodies at 4°C, slices were washed and incubated for 30 min with goat anti–rat coupled with 655-nm Quantum dots (Invitrogen) in PBS, 0.5% BSA, and 4% goat serum.

For visualizing chemokines, LNs were fixed for 2 h in 4% PFA and sliced to 320 μm and incubated for 2 h in PBS, 0.2% Triton X-100. CCL21 visualization was done by incubating slices overnight with goat anti–mouse CCL21 antibody (R&D Systems) diluted in PBS, 4% rabbit serum. Specificity of the CCL21 staining was tested by adding recombinant chemokine to a concentration of 1 μg/ml. For CXCL12 detection, slices were incubated overnight with biotinylated mouse anti–human and –mouse CXCL12 (K15C) diluted in PBS, 4% mouse serum. This antibody was provided by F. Bachelerie (45). Specificity of the CXCL12 staining was tested by preincubating LN slices with nonbiotinylated K15C. Primary antibodies were revealed with rabbit anti–goat and streptavidin coupled with 655-nm Quantum dots. All antibodies were used at a concentration of 10 μg/ml.

Chemotaxis assays. Chemotaxis assays were performed by using a transwell chamber, as previously described (46).

Statistics. Data are expressed as means ± SD, and significant differences between two series of results were assessed using the unpaired Student's *t* test. $P < 0.05$ was considered significant.

Online supplemental material. Fig. S1 shows the localization of immobile T cells within LN slices. Fig. S2 shows the time needed for PTX to inhibit CCL19-induced T cell polarization. Fig. S3 shows the fraction of memory and activated T cells recruited into LN slices in the absence of CCR7 or its ligands. Fig. S4 shows the localization of CCL21 and CXCL12 within LN slices. Fig. S5 shows that a proportion of WMN-treated T cells accumulated in HEVs after adoptive transfer. Video 1 shows the distribution of AKT-PH-GFP in migrating human T cells plated on ICAM-1 and stimulated with CCL19. Video 2 shows the basal motility of mouse T cells within a LN slice. Video 3 shows antigen-independent Ca^{2+} responses recorded in a LN slice. Video 4 shows the reduced motility of PTX-treated T cells (red) relative to control cells (green) in a LN slice. Video 5 shows the distribution and motility of CCR7-deficient T cells (red) relative to WT cells (green). Video 6 depicts the similar motilities of WMN-treated (red) and control (green) cells added to a LN slice. Video 7 shows the distribution and motility of WMN-treated T cells (red) relative to control T cells (green) within a LN slice after adoptive transfer. Online supplemental material is available at http://www.jem.org/cgi/content/full/jem.20062079/DC1.

We wish to thank Dr M. Lipp for kindly proving CCR7-deficient mice, Dr H. Nakano for kindly providing *plt/plt* mice, Dr F. Bachelerie for reagents, Dr S. Dieudonné for his help during the initiation of this project, P. Bourdoncle for advice and assistance with microscopes, C. Grolleau for help in data analysis, and Dr D. Fruman for valuable discussions.

This work was supported by grants from the Centre National de la Recherche Scientifique, the Institut National de la Santé et de la Recherche Médicale, the Ligue Nationale Contre le Cancer, and the Ministère de l'Education Nationale et de la Recherche. E. Real is a student in the Gulbenkian PhD Program in Biomedicine and was supported by the Fundação para a Ciência e a Tecnologia.

The authors have no conflicting financial interests.

Note added in proof: Similar data showing a CCR7-dependent T cell motility in the lymph node have recently been reported by Okada, T., and J.G. Cyster. 2007. *J. Immunol.* 178:2973–2978, and by Worbs, T., T.R. Mempel, J. Bolter, U.H. von Andrian, and R. Forster. 2007. *J. Exp. Med.* 204:489–495.

Submitted: 28 September 2006
Accepted: 9 April 2007

REFERENCES

1. Gunn, M.D., K. Tangemann, C. Tam, J.G. Cyster, S.D. Rosen, and L.T. Williams. 1998. A chemokine expressed in lymphoid high endothelial venules promotes the adhesion and chemotaxis of naive T lymphocytes. *Proc. Natl. Acad. Sci. USA.* 95:258–263.
2. Cyster, J.G. 2005. Chemokines, sphingosine-1-phosphate, and cell migration in secondary lymphoid organs. *Annu. Rev. Immunol.* 23:127–159.
3. Nakano, H., S. Mori, H. Yonekawa, H. Nariuchi, A. Matsuzawa, and T. Kakiuchi. 1998. A novel mutant gene involved in T-lymphocyte-specific homing into peripheral lymphoid organs on mouse chromosome 4. *Blood.* 91:2886–2895.
4. Forster, R., A. Schubel, D. Breitfeld, E. Kremmer, I. Renner-Muller, E. Wolf, and M. Lipp. 1999. CCR7 coordinates the primary immune response by establishing functional microenvironments in secondary lymphoid organs. *Cell.* 99:23–33.
5. Bousso, P., and E. Robey. 2003. Dynamics of CD8+ T cell priming by dendritic cells in intact lymph nodes. *Nat. Immunol.* 4:579–585.
6. Miller, M.J., A.S. Hejazi, S.H. Wei, M.D. Cahalan, and I. Parker. 2004. T cell repertoire scanning is promoted by dynamic dendritic cell behavior and random T cell motility in the lymph node. *Proc. Natl. Acad. Sci. USA.* 101:998–1003.
7. Bajenoff, M., J.G. Egen, L.Y. Koo, J.P. Laugier, F. Brau, N. Glaichenhaus, and R.N. Germain. 2006. Stromal cell networks regulate lymphocyte entry, migration, and territoriality in lymph nodes. *Immunity.* 25:989–1001.
8. Mempel, T.R., T. Junt, and U.H. von Andrian. 2006. Rulers over randomness: stroma cells guide lymphocyte migration in lymph nodes. *Immunity.* 25:867–869.
9. Han, S.B., C. Moratz, N.N. Huang, B. Kelsall, H. Cho, C.S. Shi, O. Schwartz, and J.H. Kehrl. 2005. Rgs1 and Gnai2 regulate the entrance of B lymphocytes into lymph nodes and B cell motility within lymph node follicles. *Immunity.* 22:343–354.
10. Kaiser, A., E. Donnadieu, J.P. Abastado, A. Trautmann, and A. Nardin. 2005. CC chemokine ligand 19 secreted by mature dendritic cells increases naive T cell scanning behavior and their response to rare cognate antigen. *J. Immunol.* 175:2349–2356.
11. Ridley, A.J., M.A. Schwartz, K. Burridge, R.A. Firtel, M.H. Ginsberg, G. Borisy, J.T. Parsons, and A.R. Horwitz. 2003. Cell migration: integrating signals from front to back. *Science.* 302:1704–1709.
12. Sun, C.X., G.P. Downey, F. Zhu, A.L. Koh, H. Thang, and M. Glogauer. 2004. Rac1 is the small GTPase responsible for regulating the neutrophil chemotaxis compass. *Blood.* 104:3758–3765.
13. Srinivasan, S., F. Wang, S. Glavas, A. Ott, F. Hofmann, K. Aktories, D. Kalman, and H.R. Bourne. 2003. Rac and Cdc42 play distinct roles in regulating PI(3,4,5)P3 and polarity during neutrophil chemotaxis. *J. Cell Biol.* 160:375–385.
14. Reif, K., K. Okkenhaug, T. Sasaki, J.M. Penninger, B. Vanhaesebroeck, and J.G. Cyster. 2004. Cutting edge: differential roles for phosphoinositide

3-kinases, p110gamma and p110delta, in lymphocyte chemotaxis and homing. *J. Immunol.* 173:2236–2240.
15. Nombela-Arrieta, C., R.A. Lacalle, M.C. Montoya, Y. Kunisaki, D. Megias, M. Marques, A.C. Carrera, S. Manes, Y. Fukui, A.C. Martinez, and J.V. Stein. 2004. Differential requirements for DOCK2 and phosphoinositide-3-kinase gamma during T and B lymphocyte homing. *Immunity.* 21:429–441.
16. Harriague, J., and G. Bismuth. 2002. Imaging antigen-induced PI3K activation in T cells. *Nat. Immunol.* 3:1090–1096.
17. Haugh, J.M., F. Codazzi, M. Teruel, and T. Meyer. 2000. Spatial sensing in fibroblasts mediated by 3′ phosphoinositides. *J. Cell Biol.* 151:1269–1280.
18. Fabre, S., V. Lang, J. Harriague, A. Jobart, T.G. Unterman, A. Trautmann, and G. Bismuth. 2005. Stable activation of phosphatidylinositol 3-kinase in the T cell immunological synapse stimulates Akt signaling to FoxO1 nuclear exclusion and cell growth control. *J. Immunol.* 174:4161–4171.
19. Sadhu, C., B. Masinovsky, K. Dick, C.G. Sowell, and D.E. Staunton. 2003. Essential role of phosphoinositide 3-kinase delta in neutrophil directional movement. *J. Immunol.* 170:2647–2654.
20. Okkenhaug, K., and B. Vanhaesebroeck. 2003. PI3K in lymphocyte development, differentiation and activation. *Nat. Rev. Immunol.* 3:317–330.
21. Rossman, K.L., C.J. Der, and J. Sondek. 2005. GEF means go: turning on RHO GTPases with guanine nucleotide-exchange factors. *Nat. Rev. Mol. Cell Biol.* 6:167–180.
22. Woscholski, R., R. Dhand, M.J. Fry, M.D. Waterfield, and P.J. Parker. 1994. Biochemical characterization of the free catalytic p110 alpha and the complexed heterodimeric p110 alpha.p85 alpha forms of the mammalian phosphatidylinositol 3-kinase. *J. Biol. Chem.* 269:25067–25072.
23. Arrieumerlou, C., and T. Meyer. 2005. A local coupling model and compass parameter for eukaryotic chemotaxis. *Dev. Cell.* 8:215–227.
24. Bhakta, N.R., D.Y. Oh, and R.S. Lewis. 2005. Calcium oscillations regulate thymocyte motility during positive selection in the three-dimensional thymic environment. *Nat. Immunol.* 6:143–151.
25. Donnadieu, E., G. Bismuth, and A. Trautmann. 1994. Antigen recognition by helper T cells elicits a sequence of distinct changes of their shape and intracellular calcium. *Curr. Biol.* 4:584–595.
26. Lo, C.G., Y. Xu, R.L. Proia, and J.G. Cyster. 2005. Cyclical modulation of sphingosine-1-phosphate receptor 1 surface expression during lymphocyte recirculation and relationship to lymphoid organ transit. *J. Exp. Med.* 201:291–301.
27. Donzella, G.A., D. Schols, S.W. Lin, J.A. Este, K.A. Nagashima, P.J. Maddon, G.P. Allaway, T.P. Sakmar, G. Henson, E. De Clercq, and J.P. Moore. 1998. AMD3100, a small molecule inhibitor of HIV-1 entry via the CXCR4 co-receptor. *Nat. Med.* 4:72–77.
28. Crump, M.P., J.H. Gong, P. Loetscher, K. Rajarathnam, A. Amara, F. Arenzana-Seisdedos, J.L. Virelizier, M. Baggiolini, B.D. Sykes, and I. Clark-Lewis. 1997. Solution structure and basis for functional activity of stromal cell-derived factor-1; dissociation of CXCR4 activation from binding and inhibition of HIV-1. *EMBO J.* 16:6996–7007.
29. Tanabe, S., Z. Lu, Y. Luo, E.J. Quackenbush, M.A. Berman, L.A. Collins-Racie, S. Mi, C. Reilly, D. Lo, K.A. Jacobs, and M.E. Dorf. 1997. Identification of a new mouse beta-chemokine, thymus-derived chemotactic agent 4, with activity on T lymphocytes and mesangial cells. *J. Immunol.* 159:5671–5679.
30. Luther, S.A., H.L. Tang, P.L. Hyman, A.G. Farr, and J.G. Cyster. 2000. Coexpression of the chemokines ELC and SLC by T zone stromal cells and deletion of the ELC gene in the plt/plt mouse. *Proc. Natl. Acad. Sci. USA.* 97:12694–12699.
31. Nolte, M.A., J.A. Belien, I. Schadee-Eestermans, W. Jansen, W.W. Unger, N. van Rooijen, G. Kraal, and R.E. Mebius. 2003. A conduit system distributes chemokines and small blood-borne molecules through the splenic white pulp. *J. Exp. Med.* 198:505–512.
32. Katakai, T., T. Hara, J.H. Lee, H. Gonda, M. Sugai, and A. Shimizu. 2004. A novel reticular stromal structure in lymph node cortex: an immuno-platform for interactions among dendritic cells, T cells and B cells. *Int. Immunol.* 16:1133–1142.
33. Hargreaves, D.C., P.L. Hyman, T.T. Lu, V.N. Ngo, A. Bidgol, G. Suzuki, Y.R. Zou, D.R. Littman, and J.G. Cyster. 2001. A coordinated change in chemokine responsiveness guides plasma cell movements. *J. Exp. Med.* 194:45–56.
34. Ward, S.G. 2004. Do phosphoinositide 3-kinases direct lymphocyte navigation? *Trends Immunol.* 25:67–74.
35. Wang, F., P. Herzmark, O.D. Weiner, S. Srinivasan, G. Servant, and H.R. Bourne. 2002. Lipid products of PI(3)Ks maintain persistent cell polarity and directed motility in neutrophils. *Nat. Cell Biol.* 4:513–518.
36. Merlot, S., and R.A. Firtel. 2003. Leading the way: Directional sensing through phosphatidylinositol 3-kinase and other signaling pathways. *J. Cell Sci.* 116:3471–3478.
37. Funamoto, S., K. Milan, R. Meili, and R.A. Firtel. 2001. Role of phosphatidylinositol 3′ kinase and a downstream pleckstrin homology domain–containing protein in controlling chemotaxis in dictyostelium. *J. Cell Biol.* 153:795–810.
38. Fukui, Y., O. Hashimoto, T. Sanui, T. Oono, H. Koga, M. Abe, A. Inayoshi, M. Noda, M. Oike, T. Shirai, and T. Sasazuki. 2001. Haematopoietic cell-specific CDM family protein DOCK2 is essential for lymphocyte migration. *Nature.* 412:826–831.
39. Sanui, T., A. Inayoshi, M. Noda, E. Iwata, J.V. Stein, T. Sasazuki, and Y. Fukui. 2003. DOCK2 regulates Rac activation and cytoskeletal reorganization through interaction with ELMO1. *Blood.* 102:2948–2950.
40. Fulga, T.A., and P. Rorth. 2002. Invasive cell migration is initiated by guided growth of long cellular extensions. *Nat. Cell Biol.* 4:715–719.
41. Park, K.C., F. Rivero, R. Meili, S. Lee, F. Apone, and R.A. Firtel. 2004. Rac regulation of chemotaxis and morphogenesis in *Dictyostelium*. *EMBO J.* 23:4177–4189.
42. Sasaki, A.T., C. Chun, K. Takeda, and R.A. Firtel. 2004. Localized Ras signaling at the leading edge regulates PI3K, cell polarity, and directional cell movement. *J. Cell Biol.* 167:505–518.
43. Revy, P., M. Sospedra, B. Barbour, and A. Trautmann. 2001. Functional antigen-independent synapses formed between T cells and dendritic cells. *Nat. Immunol.* 2:925–931.
44. Broxmeyer, H.E., C.M. Orschell, D.W. Clapp, G. Hangoc, S. Cooper, P.A. Plett, W.C. Liles, X. Li, B. Graham-Evans, T.B. Campbell, et al. 2005. Rapid mobilization of murine and human hematopoietic stem and progenitor cells with AMD3100, a CXCR4 antagonist. *J. Exp. Med.* 201:1307–1318.
45. Pablos, J.L., A. Amara, A. Bouloc, B. Santiago, A. Caruz, M. Galindo, T. Delaunay, J.L. Virelizier, and F. Arenzana-Seisdedos. 1999. Stromal-cell derived factor is expressed by dendritic cells and endothelium in human skin. *Am. J. Pathol.* 155:1577–1586.
46. Real, E., A. Kaiser, G. Raposo, A. Amara, A. Nardin, A. Trautmann, and E. Donnadieu. 2004. Immature dendritic cells (DCs) use chemokines and intercellular adhesion molecule (ICAM)-1, but not DC-specific ICAM-3-grabbing nonintegrin, to stimulate CD4+ T cells in the absence of exogenous antigen. *J. Immunol.* 173:50–60.